COMMUNICATION

Two-dimensional lead-free hybrid perovskite semiconductor with reduced melting temperature

Received 00th January 20xx,
Accepted 00th January 20xx

DOI: 10.1039/x0xx00000x

Akash Singh, [a,b] Ethan Crace, [a] Yi Xie, [a,b] and David B. Mitzi [a,c]

1-Methylhexylammonium tin iodide yields the lowest reported melting temperature (T_m=142°C) to date among lead-free hybrid perovskite semiconductors. Molecular branching near the organic ammonium group coupled with tuning of metal/halogen character suppresses T_m and facilitates effective melt-based deposition of films with 568 nm absorption onset.

Hybrid metal halide perovskites (MHPs) are a well-celebrated semiconductor family with wide ranging structure and property tunability.[1] The rich compositional space available across a range of structural dimensionalities has engendered interesting properties, contributing to the momentous growth in the fields of materials,[2] opto-electronics,[3] and photonics.[4] These advances have resulted in highly efficient solar cells,[5] light emitters,[6] and sensors.[7] Deposition techniques involving solution processing and vapor routes have been widely employed to prepare high-quality crystalline films of MHPs.[8] However, the use of toxic solvents[9] and power-intensive vacuum systems[10] towards deposition of lead-based MHPs,[11] pose health and environmental concerns. On the other hand, melt-based deposition provides an alternate solvent- and vacuum-free route to deposit MHP films,[12, 13] which can be extended to lead-free systems.[12-14] One-step melt deposition also circumvents the need for extra encapsulating agents, typically used to facilitate film/device lamination or in the fabrication of bi-facial optoelectronic devices.[15] Furthermore, application of thermal gradients may offer an additional degree of freedom to control the size/orientation of crystalline domains of the deposited film on the substrate of choice.[16] To make use of the facile and cost-effective melt-processing technique, it is imperative to design MHPs that melt (T_m) congruently and below the corresponding decomposition temperature (T_d) in order to avoid the egress of the volatile organic and hydrogen halide components[12, 17-19] as well as to establish a protocol for testing the stability of the melt.

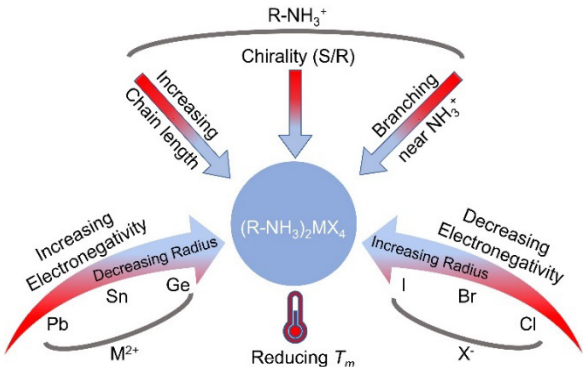

Scheme 1. *Representation of the synthetic design rules employed to reduce the melting temperature (T_m) of 2D hybrid metal halide perovskites. The change of colour from red to blue highlights the typical direction of decreasing T_m.*

Out of the colossal array of possible compositional combinations for MHPs, relatively few 2-dimensional (2D) MHPs with a general chemical formula of $(R\text{-}NH_3)_2MX_4$ (where R is an aliphatic/aromatic molecule, M is a divalent metal cation, and X is a halide anion)[2] have been previously demonstrated to show $T_m < T_d$.[12-14, 16, 19-22] To target the challenge associated with $T_m < T_d$, careful selection of R, M^{2+}, and X^- must be made. Though the identification of factors underlying or a mechanism of melting are not clearly understood even for simpler alkali halides,[23] the electronegativity and ionic radius have profound effect on the interionic interaction that effects the physical properties of metal halides[24] and ionic liquids.[25] 2D Ruddleson Popper MHPs follow an empirical correlation (Scheme 1) that allows T_m to be reduced by (i) decreasing the electronegativity of X^- (or increasing the ionic size) i.e., moving down the halide (X) group from Cl, Br, to I,[12] and (ii) increasing the metal atom electronegativity (or decreasing the ionic size), i.e., moving up the metallic group from Pb, Sn, to Ge.[21] Introducing branching near the ammonium tethering group on longer aliphatic organic chains is also a direct approach to reduce the T_m of MHPs,[12] and incorporating chiral organic cations into the MHP framework has been shown to substantially reduce the T_m to a low of 175 °C for a lead bromide-based MHP, presumably due to imparted asymmetric hydrogen bonding characteristics.[19,20] A

[a.] *Department of Mechanical Engineering and Materials Science, Duke University, Durham, North Carolina 27708, United States.*
[b.] *University program in Materials Science and Engineering, Duke University, Durham, North Carolina 27708, United States.*
[c.] *Department of Chemistry, Duke University, Durham, North Carolina 27708, United States.*

† Electronic Supplementary Information (ESI) available: Methods, Tables for crystallographic data, additional figures of crystals, X-ray diffraction pattern, crystal structure, DSC, TGA data, and images of melt processed films. CCDC 2255223 and 2255224. See DOI: 10.1039/x0xx00000x

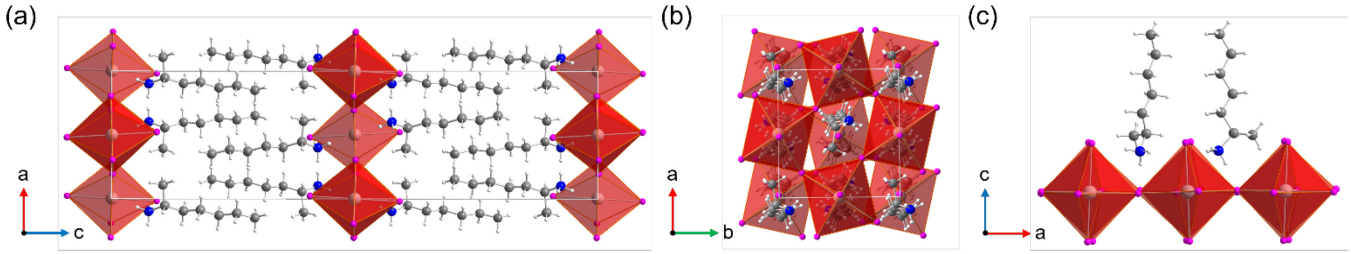

Figure 1. *Schematic side-view (**a**) and top-view (**b**) single-crystal structure of 1-MeHa$_2$SnI$_4$ at 80K. (**c**) Orientation/conformations of 1-MeHa cations, highlighting the alternating arrangement of the two enantiomers. Red, purple, grey, dark blue, and white spheres denote Sn, I, C, N, and H atoms respectively.*

recent report demonstrated a remarkably low T_m = 126 °C for a lead-iodide based MHP ((GABA)$_2$PbI$_4$, GABA$^+$: 4-ammoniumbutyric acid cation) and pointed to the possible role of O···H—O hydrogen bonds in lowering T_m.[22] Nevertheless, to the best of our knowledge, the lowest T_m reported so far for a lead-free MHP is ~170 °C, as offered by ß-methylphenethylammonium tin iodide (ß-MePEA$_2$SnI$_4$).[14] Seeking further reduction in T_m in the lead-free halide perovskite family, we targeted a low-T_m iodide-based MHP composition by combining several approaches— i.e., increased electronegativity (reduced size) of Sn (compared to Pb), focusing on less electronegative I (compared to Br), as well as use of a branched and longer organic spacer cation such as 1-methylhexylammonium.[12]

Cooling a supersaturated solution containing the 1-methylhexyamine (1-MeHa) and SnI$_2$ precursors within an aqueous hydriodic solution in a water-bath (see Methods) results in the precipitation of orange-red crystals (Figure S1). Unless otherwise stated, the prepared material was handled under N$_2$ to avoid Sn oxidation. The red-shift in the appearance of the obtained crystals as opposed to the yellowish crystals of the corresponding lead counterpart (1-MeHa$_2$PbI$_4$) hints towards the formation of the 2D MHP phase. Single crystal XRD at 80 and 300 K (Table S1) confirms that the prepared material crystallizes in a 2D perovskite structure with chemical formula of 1-MeHa$_2$SnI$_4$ and an orthorhombic space group *Pbca* with a long *c*-axis (approximately 34 Å, Figure 1a). The long *c*-axis is imparted by the interpenetration of the organic ammonium cations (1-MeHa) between perovskite layers, which causes adjacent perovskite layers to adopt a staggered geometry (Figure 1b). Additionally, the two enantiomers of the 1-MeHa cation occupy alternating lattice sites between adjacent corner-shared Sn-I octahedra (A-site hereafter), with neighbouring organic cations rotated 90° and mirrored relative to each other (Figure 1c). However, the two enantiomer sites are symmetry related in *Pbca* and result in only one crystallographically unique organic cation in the structure. Due to the high symmetry of the structure, there is only one crystallographically unique Sn cation, axial I anion, and equatorial iodide anion. The resulting tin-iodide octahedra have a nearly ideal geometry, with all trans I-Sn-I bond angles equal to 180°, all cis bond angles between 86.11-93.89°, and cis Sn-I bond distances between 3.16-3.24 Å. The largest distortion in the structure arises for the interoctahedral Sn-I-Sn bond angle, 155.72°, with all distortion occurring in the plane of the tin ions (Figure 1b). This bond angle is affected by the hydrogen bonding interactions between the nearest iodide anions with the ammonium cation and steric interaction between the methyl moiety and the inorganic lattice, which forces the ammonium cation to be off-center in the A-site. This off-centering of the cation mediates the in-plane distortion observed in the inorganic layers (Figure 1b). We also directly compared the room temperature crystal structure of 1-MeHa$_2$SnI$_4$ with the corresponding lead counterpart (1-MeHa$_2$PbI$_4$), which has been previously reported to have a low T_m (T_m = 172 °C).[12] Evaluation of the H-bonding strength[26] (known to directly impact the T_m)[27] through measurement of H-bond lengths and angles shows that both the 1-MeHa$_2$SnI$_4$ and 1-MeHa$_2$PbI$_4$ (Table S2) systems possess similar H-bonding motif and strength (Figure S2). Thus, the impact of the organic-inorganic H-bonding interactions on melting properties should be similar within these two systems. Also, both the systems show similar penetration depths of the organoammonium cations into the inorganic metal-iodide cavity (0.532 Å for 1-MeHa$_2$SnI$_4$ and 0.528 Å for MeHa$_2$PbI$_4$) which further indicates the structural similarity between the two systems (Figure S2). Notably, the discussion of H-bonding should be considered tentative, given that the H atoms are placed at idealized positions (relative to nitrogen) and the positions are refined while maintaining this ideal geometry. Upon comparing the inorganic distortions between the Sn and Pb based systems, we observe similar interoctahedra distortions (*ß*, Table S3), and intraoctahedral distortions, the latter characterized by change in bond length distortion (Δd) and bond angle variance (σ^2) (See note below Table S4).[28] The M-I bond lengths and I-M-I bond angles are listed in Table S4 and the calculated values of *ß*, Δd and σ^2 for the Sn and Pb systems are 155.7°,12.10 x 10^{-5}, 9.49°^{2} and 153.9°, 7.87 x 10^{-5}, 10.64°^{2}, respectively.

Differential scanning calorimetry (DSC, Figure 2) performed on the 1-MeHa$_2$SnI$_4$ crystals identified a structural transition (T_s = 61.4 °C) followed by congruent melting (T_m = 142.3 °C) upon heating. On cooling, the sample quickly crystallizes (T_c = 141.9 °C) near T_m with sharp onset (almost a vertical line) and insignificant degree of supercooling (0.4 °C), before finally reverting to the room temperature phase according to the structural transition (T_s = 49.3 °C) (with some hysteretic behaviour being observed). Although it is likely not possible to directly correlate the differences in T_m with distinct room-temperature structures, given prospective structural transitions before melting (often driven by order-disorder transitions of the organoammonium cations[21]), the ~30°C difference in T_m between Pb- and Sn-based systems may originate from the inorganic lattice itself. Comparisons among the intra-octahedral distortions of other available pairs of Sn and Pb iodide perovskites with common organic cations (Table S5) reveal no clear correlation between room-temperature Δd and σ^2 with T_m, suggesting insignificant direct

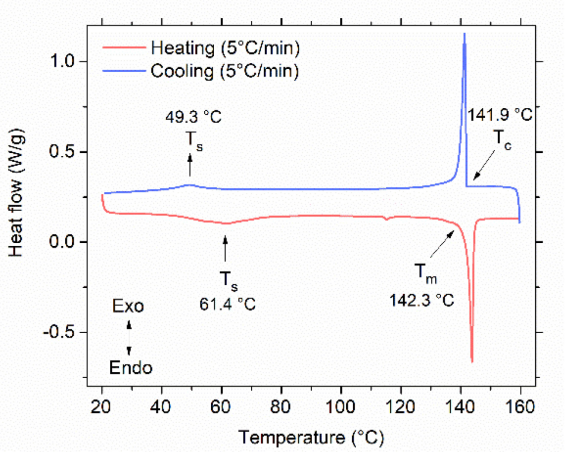

Figure 2. *Differential scanning calorimetry (DSC) measurement of 1-MeHa$_2$SnI$_4$ crystals performed under heating and cooling rates of 5 °C/min. On heating, the crystals undergo an endothermic structural (solid-solid, T_s) transition before melting (solid-liquid, T_m). During cooling, an exothermic crystallization (T_c) peak is observed, which is followed by reversal of the structural transition.*

contribution of these parameters (and therefore with the metal lone pair stereoactivity) towards a generic trend of the melting temperature difference between Sn and Pb MHPs (typically, ΔT_m = 25-45 °C). The inter-octahedra distortions (*ß*) are also found to be similar, with very small difference across various compositions of Sn and Pb MHPs (Table S5). Similarly, the penetration depths of the organoammonium cations into the inorganic layer do not directly correlate with a trend in T_m (Table S5 and S6). However, the electronegativity (electropositivity) values follow a clear decreasing (increasing) trend as we move down the group 14 column of the periodic table (Table S6). We hypothesize that the reduced electronegativity (larger radius) of the metal imparts higher ionic character to the M-I bond (similar to replacing I with a more electronegative halogen). As a result, there could be a stronger inorganic bonding interaction, leading to an increase in T_m as one goes down the group from Ge to Pb.

To the best of our knowledge, this is the lowest recorded T_m for any lead-free MHP. Though there are reports of MHPs with $T_m < T_d$, the T_d (calculated from the onset of mass loss) is not a fixed quantity and instead is a kinetic quantity, with underlying thermodynamic signatures, which can thus be contingent on the sample's form factor and the heating rate employed during the measurement. Hence, MHPs can show partial thermal decompositions at temperatures less than the measured T_d. A practical way to investigate the partial decomposition (loss of organic components) is to track the T_m and T_c of the sample over multiple heating-cooling iterations. A change of either of these thermodynamic quantities reflects disruption in the hydrogen bonding characteristics between the MHP organic and inorganic layers, thus reflecting a partial loss of organic or hydrogen halide components. For example, multiple heat-cool scans performed on 1-MeHa$_2$PbI$_4$ with T_m ~ 170 °C shows a T_m and T_c shift to lower temperatures over three iterations (Figure S3), even though the measurement upper limit temperature is only 185 °C, which is significantly less than the determined T_d = 228 °C from

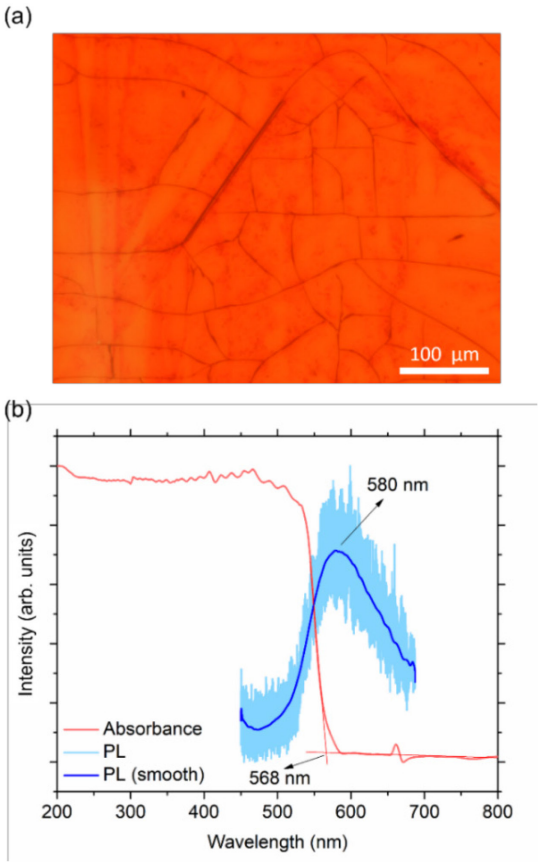

Figure 3 a. *Optical microscopy of melt-processed film of 1-MeHa$_2$SnI$_4$ sandwiched between two quartz discs.* ***b****, Optical absorbance and photoluminescence (PL) spectra of melt-processed film of 1-MeHa$_2$SnI$_4$.*

thermogravimetric analysis (TGA) measurement (Figure S4). On the other hand, over multiple heat-cool iterations performed on 1-MeHa$_2$SnI$_4$, there is no significant change in T_m and T_c, which points to the robust nature of the liquefied melt and relative avoidance of decomposition within the working temperature range (Figure S5). The robustness of the melt state circumvents the need for additional organic salt precursor to compensate for the organic/halide loss during heating,[13] which can otherwise generate electronic defect states[29] in the perovskite material during the melt-processing of 2D MHPs. Motivated by the stability of the melt state, we employed melt press-coating to fabricate a film of 1-MeHa$_2$SnI$_4$. X-ray diffraction (XRD) of the melt-processed film (see procedure #1, in Methods), obtained by melting and resolidification of the crystals, shows a primary peak at 2θ of 5.2°, with a regularly repeating pattern of (*00l*) planes, resembling the pattern shown by other 2D MHP crystals or thin-films (Figure S6).[12, 19] Due to the sensitivity of Sn to ambient moisture/oxygen, the films are also prepared in a sandwiched configuration between two quartz discs with epoxy sealing around the periphery (see procedure #2, in Methods). The low-magnification optical microscopy of the deposited film (Figure 3a) shows a smooth texture with some macroscopic cracks (developed during cooling to release thermal stress). High magnification imaging of the film, however, doesn't show any identifiable feature to suggest smaller grain size (Figure S7). Optical absorbance spectroscopy performed on the melt-processed film

shows an absorption onset of 568 nm (consistent with the orange-red color) corresponding to a bandgap of ~2.2 eV. A prospective exciton peak, expected for many 2D perovskites, is presumably missing due to saturation of the absorption spectra from the large thickness[19, 30] of the melt-processed films. However, the photoluminescence spectrum reveals a weak/broad feature at 580 nm (~2.1 eV) (Figure 3b). The absorption profile suggests prospective use of the synthesized composition in visible range optoelectronic devices; however, considering the ease of thermal processing and higher conductivity of Sn based MHPs, one could also envision their utility in low-cost melt-processed transistors.[14, 31]

In summary, we demonstrate the lowest T_m recorded for a lead-free MHP semiconductor. An iterative technique of comparing thermodynamic (such as T_m) and kinetic (such as T_d) parameters is presented as a protocol to assess the stability of the MHP melts. The single crystal structure and comparison to the analogous Pb-based system highlights the role of introduced organic cation branching near the ammonium group. When coupled with tuning the electronegative (and ionic radius) character of the metal/halogen, these features supress the T_m. The low T_m not only reduces the overall thermal budget of the melt-processing technique, but also opens an opportunity for the deposition of thin films on flexible substrates such as polyethylene terephthalate (PET) or polyethylene naphthalate (PEN) (e.g., see Figure S8), thus enabling wearable and flexible optoelectronic devices.[32] Glass formation or controlled kinetic switching in these low melting systems can also be envisioned, which could lead to cost-effective environmentally benign switching devices for memory, photonic, and spintronic applications.[19, 33] Furthermore, co-alloying the low T_m 2D MHP with 3D MHP can help extend the optical absorption regime for stable photovoltaic systems while allowing for melt processability.[13, 22]

This work was supported by the National Science Foundation under Grant No. DMR- 2114117. The work was performed in part at the Duke University Shared Materials Instrumentation Facility (SMIF), a member of the North Carolina Research Triangle Nanotechnology Network (RTNN), which is supported by the National Science Foundation (Grant ECCS-2025064) as part of the National Nanotechnology Coordinated Infrastructure.

Conflicts of interest

There are no conflicts to declare.

References

1. B. Saparov and D. B. Mitzi, *Chem. Rev.*, 2016, **116**, 4558-4596.
2. D. B. Mitzi, *Prog. Inorg. Chem.*, 1999, 1-121.
3. J. Gong, M. Flatken, A. Abate, J.-P. Correa-Baena, I. Mora-Seró, M. Saliba and Y. Zhou, *ACS Energy Lett.*, 2019, **4**, 861-865.
4. B. R. Sutherland and E. H. Sargent, *Nat. Photonics*, 2016, **10**, 295-302.
5. A. K. Jena, A. Kulkarni and T. Miyasaka, *Chem. Rev.*, 2019, **119**, 3036-3103.
6. Z. Chu, Q. Ye, Y. Zhao, F. Ma, Z. Yin, X. Zhang and J. You, *Adv. Mater.*, 2021, **33**, 2007169.
7. H. Wu, Y. Ge, G. Niu and J. Tang, *Matter*, 2021, **4**, 144-163.
8. W. A. Dunlap-Shohl, Y. Zhou, N. P. Padture and D. B. Mitzi, *Chem. Rev.*, 2018, **119**, 3193-3295.
9. G. Ding, Y. Zheng, X. Xiao, H. Cheng, G. Zhang, Y. Shi and Y. Shao, *J. Mater. Chem. A*, 2022, **10**, 8159-8171.
10. H. Li, J. Zhou, L. Tan, M. Li, C. Jiang, S. Wang, X. Zhao, Y. Liu, Y. Zhang and Y. Ye, *Sci. Adv.*, 2022, **8**, eabo7422.
11. J. Li, H.-L. Cao, W.-B. Jiao, Q. Wang, M. Wei, I. Cantone, J. Lü and A. Abate, *Nat. Commun.*, 2020, **11**, 310.
12. T. Li, W. A. Dunlap-Shohl, E. W. Reinheimer, P. Le Magueres and D. B. Mitzi, *Chem. Sci.*, 2019, **10**, 1168-1175.
13. T. Li, A. M. Zeidell, G. Findik, W. A. Dunlap-Shohl, J. Euvrard, K. Gundogdu, O. D. Jurchescu and D. B. Mitzi, *Chem. Mater.*, 2019, **31**, 4267-4274.
14. D. B. Mitzi, C. D. Dimitrakopoulos, J. Rosner, D. R. Medeiros, Z. Xu and C. Noyan, *Adv. Mater.*, 2002, **14**, 1772-1776.
15. T. Li, W. A. Dunlap-Shohl and D. B. Mitzi, *ACS Appl. Energy Mater.*, 2020, **3**, 9493-9497.
16. D. B. Mitzi, D. R. Medeiros and P. W. DeHaven, *Chem. Mater.*, 2002, **14**, 2839-2841.
17. C. C. Stoumpos, C. D. Malliakas and M. G. Kanatzidis, *Inorg. Chem.*, 2013, **52**, 9019-9038.
18. *US Pat.,* 17/333,862, 2022.
19. A. Singh, M. K. Jana and D. B. Mitzi, *Adv. Mater.*, 2021, **33**, 2005868.
20. A. Singh and D. B. Mitzi, *ACS Mater. Lett.*, 2022, **4**, 1840-1847.
21. D. B. Mitzi, *Chem. Mater.*, 1996, **8**, 791-800.
22. M. B. H. Salah, N. Mercier, S. Dabos-Seignon and C. Botta, *Angew. Chem. Int. Ed.*, 2022, **134**, e202206665.
23. A. Galwey, *J. Therm. Anal. Calorim.*, 2005, **82**, 23-40.
24. H. Kanno, *Nature*, 1968, **218**, 765-766.
25. P. Sanchora, D. K. Pandey, D. Rana, A. Materny and D. K. Singh, *J. Phys. Chem. A*, 2019, **123**, 4948-4963.
26. S. J. Grabowski, *Understanding hydrogen bonds: theoretical and experimental views*, Royal Society of Chemistry, 2020.
27. K. Fumino, T. Peppel, M. Geppert-Rybczyńska, D. H. Zaitsau, J. K. Lehmann, S. P. Verevkin, M. Köckerling and R. Ludwig, *Phys. Chem. Chem. Phys.*, 2011, **13**, 14064-14075.
28. K.-z. Du, Q. Tu, X. Zhang, Q. Han, J. Liu, S. Zauscher and D. B. Mitzi, *Inorg. Chem.*, 2017, **56**, 9291-9302.
29. C. M. Perez, D. Ghosh, O. Prezhdo, W. Nie, S. Tretiak and A. Neukirch, *J. Phys. Chem. Lett.*, 2022, **13**, 5213-5219.
30. V. S. Chirvony, I. Suárez, J. Rodríguez-Romero, R. Vázquez-Cárdenas, J. Sanchez-Diaz, A. Molina-Sánchez, E. M. Barea, I. Mora-Seró and J. P. Martínez-Pastor, *ACS Appl. Nano Mater.*, 2021, **4**, 6170-6177.
31. A. Liu, H. Zhu, S. Bai, Y. Reo, T. Zou, M.-G. Kim and Y.-Y. Noh, *Nat. Electron.*, 2022, **5**, 78-83.
32. R. Zhao, Z. Gu, P. Li, Y. Zhang and Y. Song, *Adv. Mater. Technol.*, 2022, **7**, 2101124.
33. Y. Xie, R. Song, A. Singh, M. K. Jana, V. Blum and D. B. Mitzi, *J. Am. Chem. Soc.*, 2022, **144**, 15223-15235.

